Journal of Materials Science & Technology 62 (2021) 83–95

Contents lists available at ScienceDirect

Journal of Materials Science & Technology

journal homepage: www.jmst.org

Research Article

Photothermy-strengthened photocatalytic activity of polydopamine-modified metal-organic frameworks for rapid therapy of bacteria-infected wounds

Donglin Han[a], Yuan Li[a], Xiangmei Liu[b,*], Kelvin Wai Kwok Yeung[c], Yufeng Zheng[d], Zhenduo Cui[a], Yanqin Liang[a], Zhaoyang Li[a], Shengli Zhu[a], Xianbao Wang[b], Shuilin Wu[a,*]

[a] School of Materials Science & Engineering, The Key Laboratory of Advanced Ceramics and Machining Technology by the Ministry of Education of China, Tianjin University, Tianjin 300072, China
[b] Hubei Collaborative Innovation Center for Advanced Organic Chemical Materials, Ministry-of-Education Key Laboratory for the Green Preparation and Application of Functional Materials, Hubei Key Laboratory of Polymer Materials, School of Materials Science & Engineering, Hubei University, Wuhan 430062, China
[c] Department of Orthopaedics & Traumatology, Li Ka Shing Faculty of Medicine, The University of Hong Kong, Pokfulam, Hong Kong 999077, China
[d] State Key Laboratory for Turbulence and Complex System and Department of Materials Science and Engineering, College of Engineering, Peking University, Beijing 100871, China

ARTICLE INFO

Article history:
Received 17 April 2020
Received in revised form 8 May 2020
Accepted 21 May 2020
Available online 9 July 2020

Keywords:
Metal-organic framework
Photosensitizer
Antibacterial
Photothermal
Wound healing

ABSTRACT

Herein, a metal-organic framework (MOF) was modified using polydopamine (PDA) to develop the MOF-PDA as a photoresponsive bacteria-killing agent under 660 nm light irradiation. The modification using PDA led to the production of not only more heat, but also much more $^1O_2$. This is because the PDA could interact with the porphyrin ring of the MOF through π-π interaction and the charge transfer between PDA and the MOFs decreases the energy of the band of hybrid nanoparticles. In addition, greater levels of hyperthermia induced by PDA modification accelerated the charge transfer, which significantly strengthened the photocatalytic performance of MOF-PDA. Furthermore, after modification, the light absorbance and water dispersibility of nanoparticles were both enhanced; both are important for the improvement of photocatalytic and photothermal properties. Consequently, MOF-PDA exhibited the highly effective antibacterial efficacy of 99.62 % and 99.97 % against *Staphylococcus aureus* and *Escherichia coli*, respectively, under 20 min 660 nm light irradiation.

1. Introduction

To avoid bacterial infections, the most common antibacterial agents, antibiotics, have been widely used [1,2]. However, the large doses of antibiotics used gradually led to another serious problem, *i.e.*, the appearance of drug-resistance bacteria, which could be immune to traditional antibiotics, thus becoming deadly for humans again [3,4]. Hence, it is quite urgent to develop new antibacterial agents and highly efficient bacteria-killing strategies independent of antibiotics.

MOF is a kind of porous material which consists of organic linkers and metal nodes [5,6]. Because there are abundant alternative compositions, MOFs can easily be endowed with various kinds of properties easily, such as selective gas storage, H_2 evolution and CO_2 reduction [7,8]. Some research has used MOFs as antibacterial agents, with Cu, Ag, and Zn commonly used as nodes [9,10], for example, CuBTC or Ag_3(3-phosphonobenzoate), releases metallic ions that can kill bacteria. However, those cases are often accompanied by insufficient antibacterial properties or serious side effects, such as toxicity [9,10]. Because the metal ions could enter the body by penetrating through the skin, and then accumulate in organs. Recent studies have shown that some synthesized materials that include MOF [11,12], which could produce free radical and heat under light irradiation, could be employed as effective antibacterial agents. Among them, the MOF PCN 224 with Zr_6 clusters and meso-Tetra(4-carboxyphenyl)porphine (H_4TCPP), is attractive

* Corresponding authors.
E-mail addresses: liuxiangmei1978@163.com (X. Liu), shuilinwu@tju.edu.cn (S. Wu).

https://doi.org/10.1016/j.jmst.2020.05.055
1005-0302/

[13,14], due to its ability to produce $^1O_2$ and heat under 660 nm light irradiation as well as its high stability and good biocompatibility [15–18]. However, the poor photothermal properties of the MOF mean that the MOF is unable to efficiently kill bacteria within a short period of time, and singlet oxygen produced is insufficient to kill the bacteria. Polydopamine (PDA) is a kind of highly biocompatible material which has been widely used in the field of biomaterials [19,20]. Because of the large amount of π electrons that existed in PDA, it could also be used to improve materials' photocatalytic properties through the faster charge carriers transportation after modification [21]. Furthermore, PDA could also serve as a photosensitizer to transform light into heat [22,23]. With these in mind, we proposed a novel hypothesis that modifying MOFs using PDA would enhance the photocatalytic activity and photothermal effect of MOFs by accelerating the transfer of photogenerated electrons and increasing light absorption.

Thus, we synthesized a hybrid compost of MOF and PDA which possesses excellent photocatalytic activity and photothermal performance. In the hybrid MOF-PDA, the synthesized MOF was employed as the core and then modified with PDA through a simple self-polymerization method. This modification significantly improved the water dispersity and light absorbance of the MOF. Furthermore, after modification with PDA, the photothermal and photocatalytic properties of the nanoparticles were also significantly enhanced. And the enhanced photocatalytic property mainly came from the decreased energy band gap and enhanced photothermal property after PDA modification. Due to the combination of enhanced photothermal and photocatalytic properties, the antibacterial efficacy of MOF-PDA could reach up to 99.62 % and 99.97 % for *S. aureus* and *E. coli* after a 20-minute light treatment session that used wavelengths of 660 nm. More importantly, the MOF-PDA showed excellent biocompatibility, guaranteeing its potential as a suitable antibacterial agent. The *in vivo* experiments showed that the MOF-PDA possessed efficient antibacterial property with no damage to major organs.

2. Materials and methods

2.1. Synthesis of MOFs

The MOF nanocrystals were synthesized using the following process. Briefly, three kinds of components, 1.2 g of benzoic acid, 120 mg of $ZrOCl_2.8H_2O$ and 40 mg of meso-Tetra(4-carboxyphenyl)porphine (H_4TCPP) were resolved in *N,N*-Dimethylformamide (DMF), then kept at 120 °C for 24 h. Nanocrystals were collected and washed with DMF three times and dried for further use. As for the preparation of MOF-PDA nanocrystals, the previously prepared MOF nanocrystals were dispersed in tris-HCl buffer (pH = 8.4) with the help of cell shredder at the final dosage of 5 mg/mL. After that, dopamine (DA) hydrochloride was dropped until the solution reached concentration of 2 mg/mL, then it was shaken at room temperature for 12 h to obtain MOF-PDA nanoparticles.

2.2. Characterization of different nanoparticles

The morphology and elemental mapping images of MOF and MOF-PDA were characterized by the Scanning Electron Microscope (SEM, JSM-7800 F, JAPAN), Transmission Electron Microscope (TEM, JEM 2100-F, Japan). The size of the synthesized nanocrystals was characterized using dynamic light scattering analysis (DLS, Zeta-Pals Brookhaven). The chemical groups and phase structure of the MOF and MOF-PDA were characterized using Fourier Transform Infrared Spectroscopy (FTIR, AVANCE IIITM HD 400 MHz NanoBAY, China) and X-Ray Powder Diffraction (XRD, D8 Advanced, Germany). The Ultraviolet–visible spectrum (UV–vis spectrum) of prepared samples was detected using a UV–vis-NIR spectrophotometer (UV-2700, Japan) (dosage: MOF-PDA: 350 ppm; MOF: 250 ppm; PDA: 100 ppm).

2.3. Photothermal property measurement

The 200 μL of the 350 ppm MOF-PDA, 250 ppm MOF and 100 ppm PDA solution was put into a 96-well plate, respectively, and irradiated by 660 nm light (0.7 W/cm^2, the ratio among the MOF, MOF-PDA and PDA was fixed and set correlated to the content in the MOF-PDA composite according the preparation of MOF-PDA). The samples were kept under the light for 5 min, then in the dark for 5 min, and this cycle was repeated 3 times in order to verify the photothermal stability of MOF-PDA and MOF. Then, in order to test the photothermal property of the samples, 200 μL of the 350 ppm MOF-PDA, 250 ppm MOF and 100 ppm PDA solution was put into a 96-well plate, respectively, then irradiated by 660 nm light (0.7 W/cm^2) until the temperature peaked.

2.4. Photocatalytic property measurement

The three kinds of samples were mixed with 1,3-Diphenylisobenzofuran (DPBF) (50 μM, dimethyl sulfoxide as solvent) in a 96-well plate at the final dosage of MOF 25 ppm, MOF-PDA 35 ppm and PDA 10 ppm, respectively. After the samples were either exposed to light or held in the dark, the absorbance of samples was detected using a microplate reader every 10 s. To permit comparison, the corresponding samples were mixed with deionized water and treated with 660 nm light (0.7 W/cm^2) or kept in the dark. To further test the mechanism of the enhanced photocatalytic properties of MOF-PDA, the experiments were repeated in ice bath.

2.5. In vitro *antibacterial tests*

The materials and bacteria (3×10^7 CFU/mL) were mixed in a 96-well plate (final dosage: MOF-PDA 350 ppm, MOF 250 ppm, and PDA 100 ppm). Then, the solution was irradiated under 660 nm light for 20 min or kept in the dark. After that, the treated solution was diluted 100 times with culture medium, and 20 μL of the diluted solution was taken out and cultured on agar plates. After being cultured at 37 °C for 24 h, the plates were photographed and calculated.

2.6. Bacterial membrane integrity evaluation

8-anilino-1-naphthalenesulfonic acid (ANS) and o-nitrophenyl-β-D-galactopyranoside (ONPG) were used as detectors to evaluate the integrity of the bacteria membrane. For the ANS experiments, the bacterial suspension (*S. aureus, E. coli*) was centrifuged at 4 °C and diluted with phosphate buffer (PBS) until the optical density (OD) value of the solution was equal to 0.05. After that, the ANS solution was mixed with the bacterial solution at a volume ratio equal to 11:100 (ANS: bacteria). Then the mixtures were further mixed with MOF, MOF-PDA and PDA, and irradiated under 660 nm light for 20 min or kept in the dark (a final dosage of MOF, MOF-PDA and PDA was 250, 350 and 100 ppm). The solutions were tested using a microplate reader. For the ONPG experiments, the bacterial solution was mixed with the isopropyl-β-D-thiogalactopyranoside (IPTG) medium at the volume ratio equal to 1:4 and shacked at 37 °C overnight. Then, the bacterial solution was centrifuged at 4 °C and diluted with PBS until the OD value fell to between 0.05 and 0.1. After adding MOF, MOF-PDA and PDA, the solution was exposed to light with the wavelength of 660 nm or kept in dark. Then the

OD value of the solution was tested using microplate reader at a wavelength of 420 nm (BioTek, SYERGY).

The group of MOF-I, MOF-PDA-I, and PDA-I meant that the bacteria were mixed with MOF, MOF-PDA, and PDA, then irradiated with 660 nm light (0.7 W/cm^2) in an ice bath for 20 min. The MOF-L, MOF-PDA-L, and PDA-L meant that the bacteria were mixed with MOF, MOF-PDA, and PDA, and then irradiated with 660 nm light for 20 min (0.7 W/cm^2) at room temperature.

The SEM images were also taken of the bacteria following their various treatments. The nanoparticles and bacteria were mixed in a 96-well plate and exposed to 660 nm light or kept in dark. After being treated using light or being left in the dark, the mixtures were treated with 4% polyformaldehyde and 10 %, 20 %, 30 %, 40 %, 50 %, 70 %, and 90 % ethyl alcohol, respectively. After that, the 96-well plate was sprayed with gold and then observed using SEM.

2.7. In vitro *cytotoxicity of the nanoparticle tests*

Thiazolyl Blue Tetrazolium Bromide (MTT) experiment was used to test the cytotoxicity of the nanoparticles. The NIH 3T3 cells were cultured in a 96-well plate for 24 h previously, followed by the addition of MOF, MOF-PDA and PDA at a final dosage of 250 ppm, 350 ppm and 100 ppm, respectively. The medium was replaced every other day. The cells mixed with the nanoparticles were exposed to 660 nm light (0.7 W/cm^2) for 20 min or kept in the dark throughout. After culturing for either 1 or 3 days, the medium was extracted and 10 μL of the MTT solution and 90 μL of the medium were added. After culturing for 4 h at 37 °C, the solution was replaced by 200 μL dimethylsulfoxide. After centrifugation, 100 μL of supernate was extracted and tested using a microplate reader (BioTek, SYERGY).

Cell morphology was also viewed *via* fluorescence staining. The glass pieces were pre-placed in a 24-well plate, and 1 mL of cell suspension was added. After culturing for 24 h, the nanoparticles were added at dosage of 250 ppm (MOF), 350 ppm (MOF-PDA), and 100 ppm (PDA). After the nanoparticles were added, the cells were exposed to 660 nm light (0.7 W/cm^2) for 20 min or kept in the dark. After culturing at 37 °C for 1 day, the pieces were washed with PBS 3 times, and fixed using formaldehyde fixing solution and ice acetone. After that, the pieces were dyed using both Phalloidin FITC and DAPI and were observed using a laser scanning confocal microscope (BioTek, SYERGY).

2.8. In vivo *experiments*

The male rats (weight: 200–220 g) were purchased from Bei-Jing HuaFu Biotechnology Company and randomly divided into five groups. The experiments were approved by the Department of Orthopedics at Union Hospital, part of Tongji Medical College at the Huazhong University of Science and Technology in Wuhan, China. These groups were named Control, 3 M, MOF, MOF-PDA and PDA. In each group, there were 12 rats. After feeding for 2 days, the rats were narcotized, and 4 wounds with a diameter of about 17 mm were cut into their backs. Then 10 μL of *S. aureus* solution was added onto the wounds to build a wound infection model, followed by differing treatments. For the Control group, the wounds were directly covered with gauze. The 3 M group had their wounds covered with 3 M adhesive wound dressing. For the MOF group, following the addition of bacterial solution, the MOF solution was added to the wound and irradiated with 660 nm light for 20 min. The MOF-PDA group had the bacterial solution added, followed by the MOF-PDA solution, which was then irradiated with 660 nm light for 20 min. The PDA group, had bacterial solution added, then the PDA solution was added and irradiated with 660 nm light for 20 min. For MOF, MOF-PDA, and PDA, all wounds were covered with gauze following respective treatments. Wound tissues were extracted 2, 4, 8, and 12 days after treatment following the euthanasia of the rats; samples were stained using H&E.

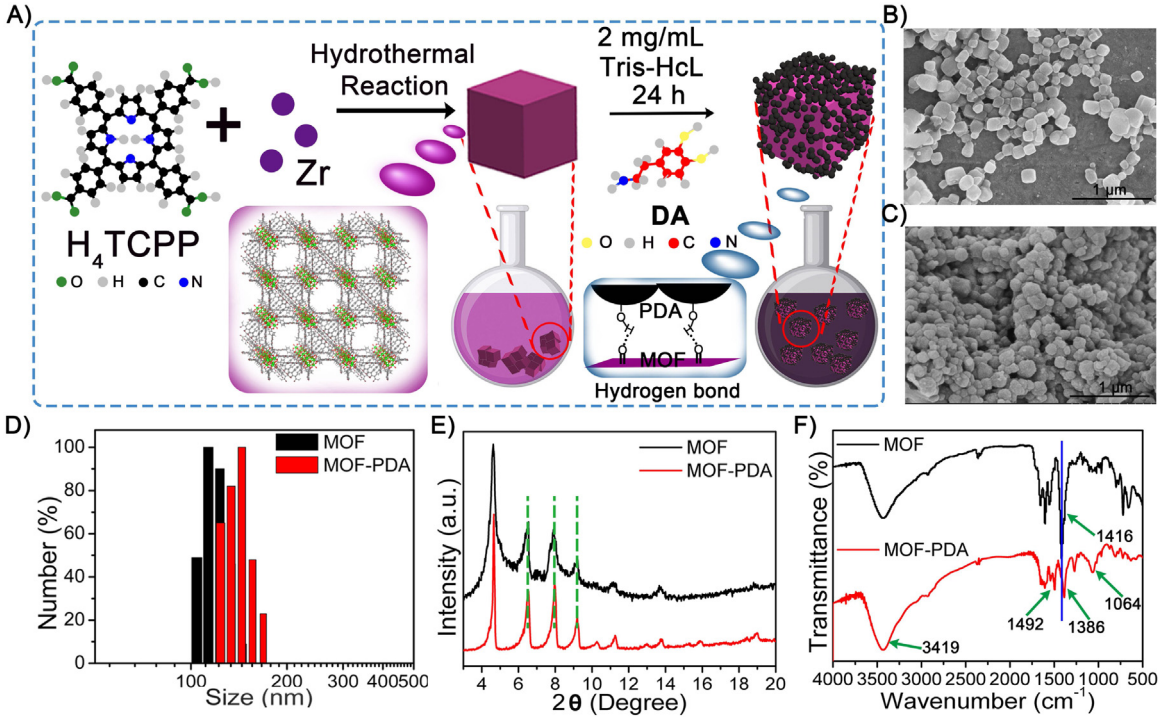

Fig. 1. Characterization of MOF and MOF-PDA. A) Schematic illustrating the process synthesizing MOF and MOF-PDA, as well as the structure of MOF and MOF-PDA, B) the SEM images of the MOF, C) the SEM images of the MOF-PDA, D) the size distribution, E) XRD spectra, F) FTIR spectra of the MOF and the MOF-PDA.

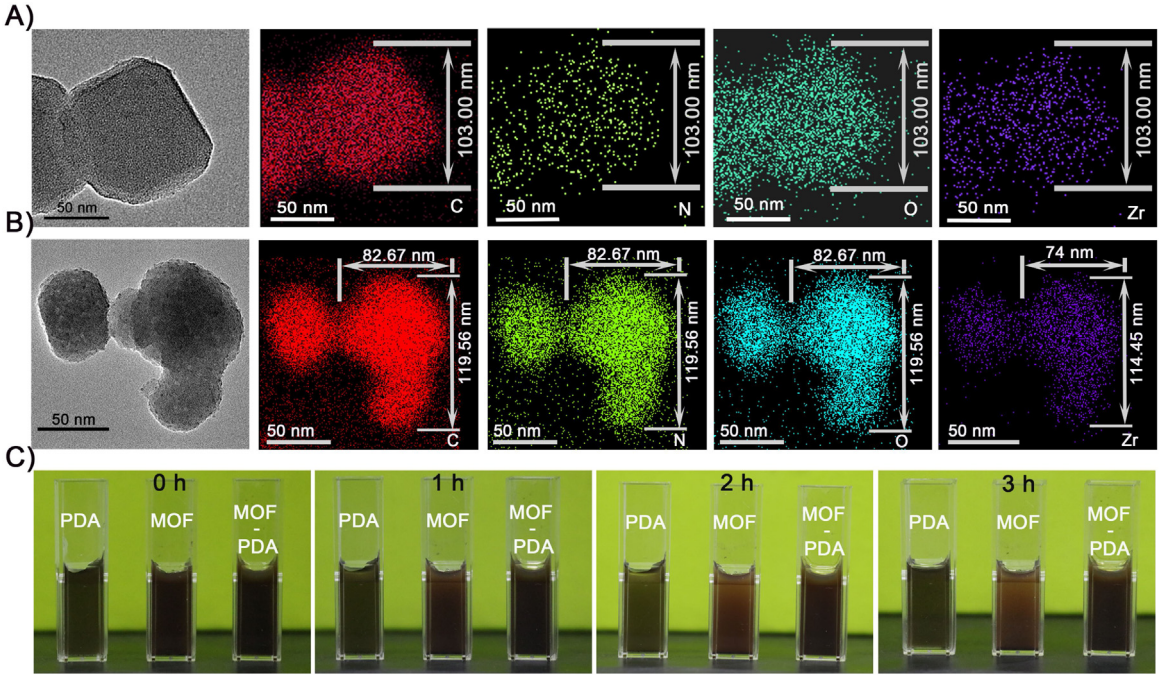

Fig. 2. The morphology and water dispersibility of MOF and MOF-PDA. The TEM image and elemental mapping images of A) MOF, B) MOF-PDA, C) the water dispersibility of MOF and MOF-PDA.

2.9. Statistical analysis

The data from all experiments were presented as averages with standard deviation (SD). Data were compared using one-way ANOVA or two-way ANOVA.

3. Results and discussion

3.1. Characterization of MOF-PDA nanoparticles

As illustrated in Fig. 1(A), the synthesized MOF consisted of Zr_6 clusters and H_4TCPP linkers. These nanoparticles were nanocubes with smooth surfaces, and they are 100–150 nm in size. Through a simple self-polymerization in the buffer, the synthesized MOF nanoparticles could be grafted by PDA on the surface through hydrogen bonding, and the schematics of this process is shown in Fig. 1(A). SEM images disclosed that the nanoparticles became rougher after surface polymerization (Fig. 1(B) and (C)). In addition, the average size of these hybrid nanoparticles was slightly larger than pure MOF (Fig. 1(D)). The XRD patterns shown in Fig. 1(E) revealed that all the peaks of MOF-PDA had the same positions as the peaks of MOF, which indicated that PDA modification did not change the structure of MOF. FTIR was used to analyze the specific binding group of MOF-PDA more precisely (Fig. 1(F)). As can be seen in Fig. 1(A), there were many O—H and NH— bonds in both MOF and PDA; it was rational to find a broad vibration band around 3500 cm^{-1} in the spectra of both MOF and MOF-PDA [24–26]. In the spectrum of MOF-PDA, there were few narrow peaks, which evidenced the polymerization of small molecular dopamine [27–29]. The two peaks between 1250 and 1500 cm^{-1} came from the phenolic C—OH— bending and stretching vibration [27,30]; the stronger peaks that appeared around 1492 cm^{-1} were attributed to the amide group's N—H shearing vibrations, and the peaks around 1064 cm^{-1} were attributed to the C—O vibrations [27], both of which indicated the presence of PDA (Fig. 1(F)). In the MOF spectrum, a strong peak at 1416 cm^{-1} could be found, which came from COO– bonds [31]. As for the MOF-PDA, this peak moved to 1386 cm^{-1} (Fig. 1(F)). This shift confirmed the formation of hydrogen bonds between the PDA coating and the MOF [32], which resulted from the abundance of amino in the PDA and the carboxyl in the porphyrin ring.

The TEM was used to further observe the morphology of the MOF and MOF-PDA. The TEM image showed that the surfaces of MOF-PDA nanoparticles were much rougher than those of MOFs (Fig. 2(A) and (B)). As shown in the elemental mapping images of the MOF, the images of elements C, N, O and Zr were all equal in size (Fig. 2(A)). However, for MOF-PDA, the images of C, N, and O were similar, and they were all larger than the Zr (Fig. 2(B)), which was due to the PDA covering the MOF nanoparticles. After ultrasonic dispersion, both MOF and MOF-PDA could form uniform turbid liquid (Fig. 2(C)). However, the dispersibility of MOF in water is poor. After 1 h, the solution began to develop multiple/distinct layers. Two hours after the starting point, the MOF solution showed obvious sediment at the bottom, with relatively clear supernate left over. Because of the great hydrophilicity of PDA, the MOF-PDA nanoparticles synthesized would disperse well in water, even after standing for hours, which also confirmed that the nanoparticles were covered by PDA.

3.2. Photothermal and photocatalytic effects

Because of the existence of H_4TCPP and PDA in MOF-PDA, it was speculated that MOF-PDA possessed the photothermal and photocatalytic properties [33–37]. Light absorbance was important for both the photothermal and photocatalytic properties of nanoparticles [38]. As shown in Figs. 3(A) and S1, both PDA and MOF exhibited low light absorbance at around 660 nm. In contrast, after the modification of PDA, light absorbance dramatically improved. This enhanced light absorbance came from several respects. First, both the H_4TCPP and PDA absorbed light due to the π–π^* transition [39,40]. Furthermore, when the MOF was covered with PDA, π–π interaction existed between the H_4TCPP and PDA, leading to the elongation of π-conjugation, which could cause splitting in the π and π^* levels, resulting in increased light absorbance and the red-shifting of the peaks [39,41], as shown in Fig. 3(A). Second, both the MOF and PDA could absorb light, so when they were combined, the light absorbance of MOF-PDA could be radically enhanced. Third, the modification using PDA remarkably improved the nanoparti-

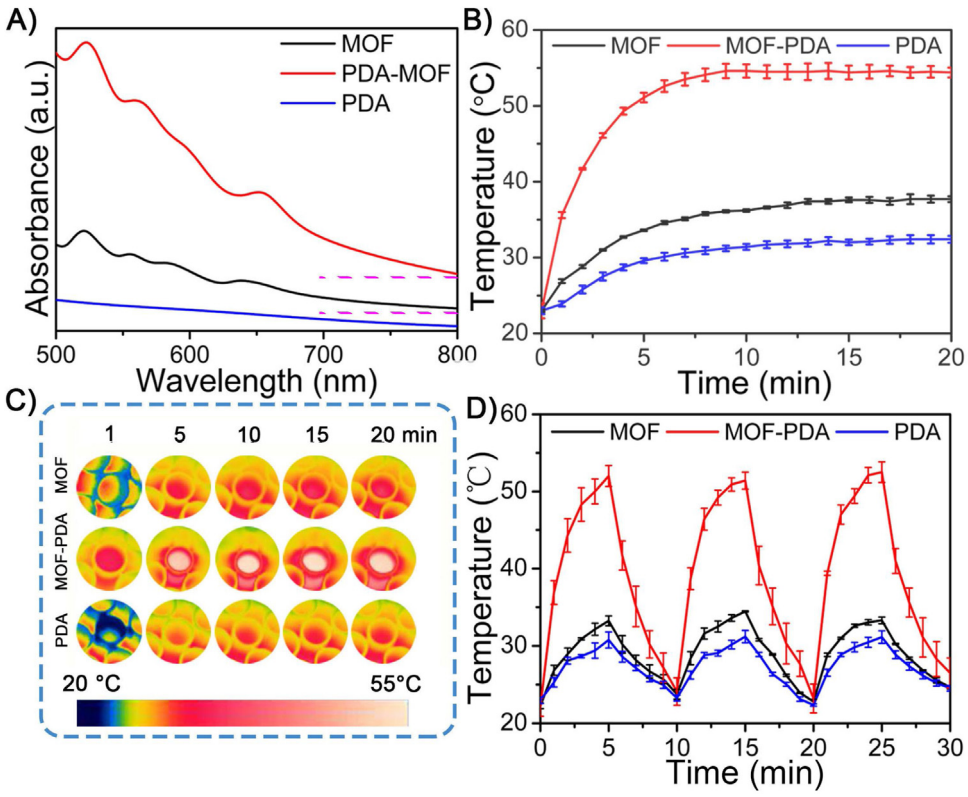

Fig. 3. The characterization of photothermal properties of MOF, PDA, and MOF-PDA. A) The UV–vis spectra of MOF, MOF-PDA, and PDA, B) the heating curves of MOF, PDA, and MOF-PDA, C) the thermal images taken during light irradiation process of MOF, MOF-PDA, and PDA, D) the heating and cooling curves of MOF, MOF-PDA, and PDA (660 nm, 0.7 W/cm^2).

cles' dispersity in water, which also enhanced the light absorbance (Fig. 2(C)).

The photothermal curves demonstrated that MOF-PDA showed a much greater ability to transform light into heat under 660 nm light irradiation, compared to either MOF or PDA alone at an equivalent dosage (Fig. 3(B) and (C)). This has three causes. First, it was evident that both PDA and MOF could produce heat under light irradiation (Fig. 3(B) and (C)). When they were combined, the ability to transform light into heat was absolutely enhanced. Furthermore, following the modification with PDA, the enhanced light absorbance at 660 nm of MOF-PDA nanoparticles could also improve the photothermal property of the nanoparticles. Finally, the modified MOF showed a much better water dispersibility, which also benefited to heat production [42]. For all of MOF, PDA, and MOF-PDA, when the light was moved away after irradiation, the temperature went down gradually, and this cycle could be repeated several times without any obvious differences, attesting to the particles' excellent photothermal stability (Fig. 3(D)).

MOF-PDA could produce not only heat but also $^1O_2$ under light irradiation. DPBF could be used to detect the photocatalytic properties of three kinds of materials. In order to avoid the influence from the MOF, MOF-PDA, PDA themselves, two groups of experiments were performed as controls. The MOF, MOF-PDA, and PDA were mixed with deionized water at equivalent dosages and then either kept in the dark or exposed to 660 nm light, and the absorption was determined every 10 s. It was clear that the absorbance did not change (Fig. S2), which indicated that the MOF, MOF-PDA, and PDA were stable in water either exposed to light or kept in the dark. Then, the MOF, MOF-PDA, and PDA were mixed with DPBF at equivalent dosage and then exposed to 660 nm light. 1 min later, the absorbance decreased by 0.684 and 0.1 at 416 nm for MOF-PDA and MOF respectively, which demonstrates that MOF-PDA could produce much more $^1O_2$ than could MOF. PDA alone could not produce $^1O_2$ at all (Fig. 4(A–C)). However, when the MOF, MOF-PDA, and PDA were mixed with DPBF and kept in the dark, the absorbance of the light did not change (Fig. 4(D–F)). The results showed that the modification of MOF nanoparticles using PDA significantly enhanced the nanoparticles' photocatalytic properties even though the PDA itself did not demonstrate any photocatalytic properties.

3.3. *Mechanism of strengthened photocatalytic properties of MOF-PDA*

Aside from improved photothermal effects, after being coated with PDA, the photocatalytic properties of nanoparticles were strongly enhanced as well. Several experiments were conducted to study the underlying mechanism. First, the UV–vis diffuse reflection was performed to calculate the energy band gap of the MOF and MOF-PDA. The results revealed that the modification of PDA decreased the energy of the nanoparticles in the band gap, as shown in Fig. 5(A). Compared against MOF, MOF-PDA presented a red-shift in the lower-energy edge of the UV–vis absorbance spectrum, indicated by the increased angle shown in Fig. 3(A), which also confirmed the decreased band gap energy [43]. Owing to the unique unsaturated ring in MOFs, π-π interaction and charge transfer could occur between PDA and H_4TCPP, which led to a shift in the HOMO and the LUMO [44,45], thus leading to the decreased energy in the band gap (Fig. 5(A)). This decreased band gap enhanced the photocatalytic property of MOF-PDA. The results of electronic impedance spectrum and photocurrent testing showed that after modification using PDA, the rate of carriers' transportation was significantly enhanced (Fig. 5(B)), and many more carriers could be produced under light irradiation (Fig. 5(C)). This was consistent with the results shown in Fig. 4. The π-π interaction and subsequent charge transfer between PDA and H_4TCPP accelerated

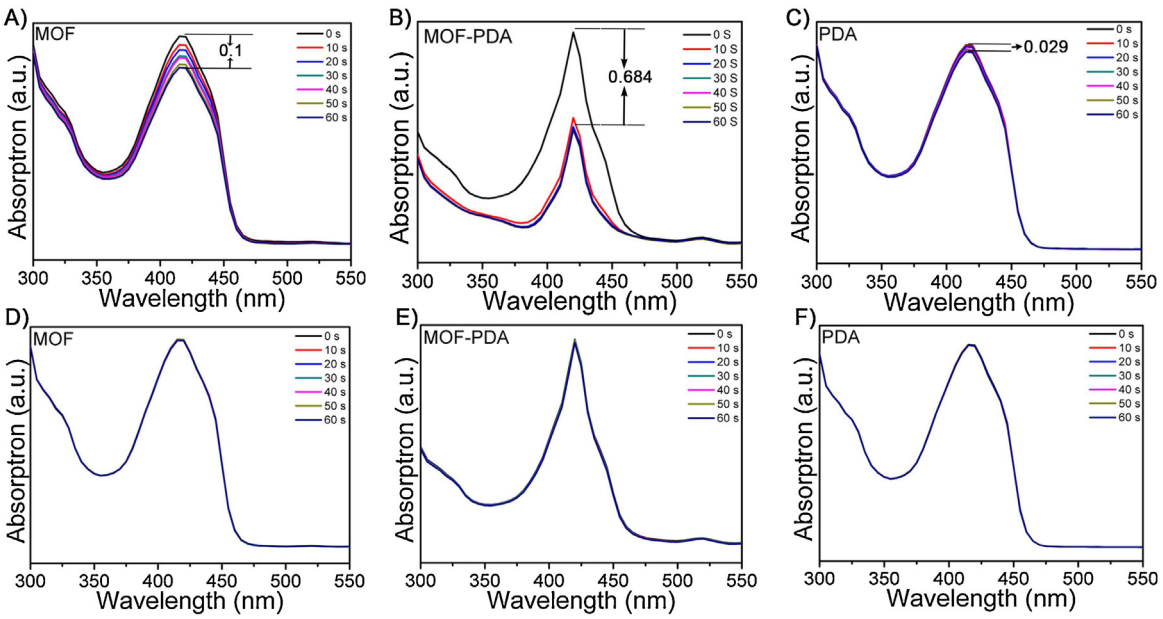

Fig. 4. The characterization of photocatalytic properties of MOF, MOF-PDA, and PDA. The detection of $^1O_2$ at room temperature using DPBF as detector under light irradiation for A) MOF, B) MOF-PDA, and C) PDA nanoparticles, the detection of $^1O_2$ at room temperature using DPBF as detector in the dark for D) MOF, E) MOF-PDA, and F) PDA nanoparticles (660 nm, 0.7 W/cm^2).

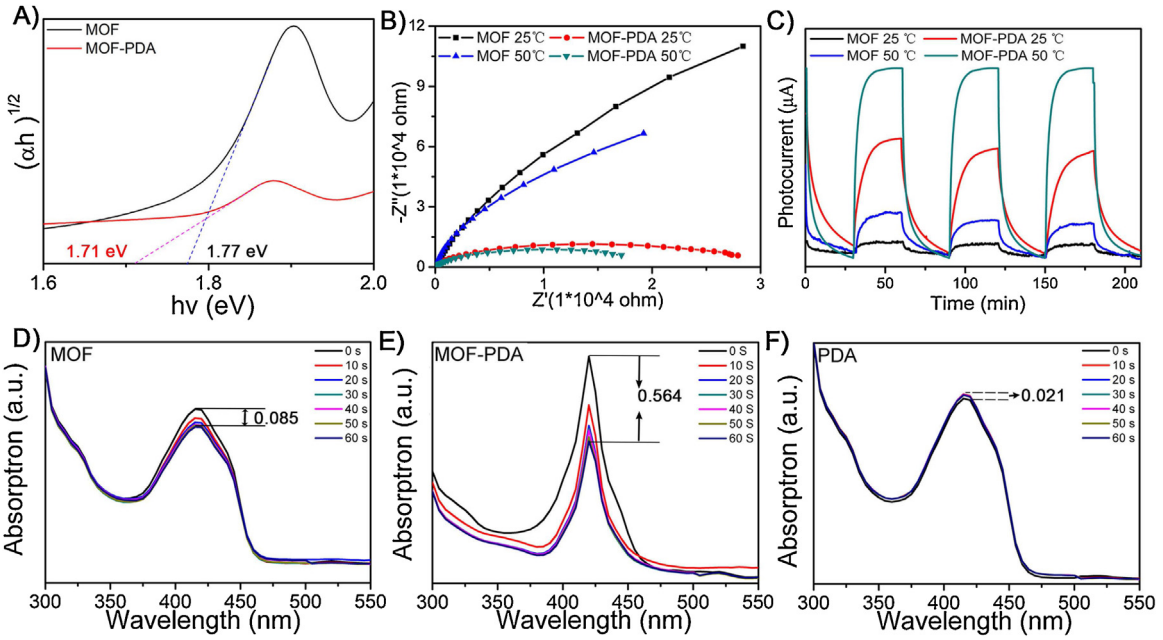

Fig. 5. The mechanism of the enhanced photocatalytic properties of MOF-PDA. A) the band energy of MOF and MOF-PDA, B) electronic impedance spectrum, C) photocurrent testing of MOF and MOF-PDA under light irradiation at different temperatures, Detection of the $^1O_2$ production with DPBF as detector under light irradiation in ice bath for D) MOF, E) MOF-PDA, F) PDA.

the carriers' transportation, greatly decreasing electrical resistance. The decreased band gap of MOF-PDA resulted in much more carriers being produced under light irradiation, which led to a significantly higher photocurrent value. Moreover, it could not be ignored that following PDA modification, much more heat could be produced under light irradiation. The electronic impedance and photocurrent testing experiments were repeated in a 50 °C water bath to test the role of heat in $^1O_2$ production. For both MOF and MOF-PDA, the resistance in transporting carriers became much smaller (Fig. 5(B)), and more carriers could be produced (as indicated by the higher photocurrent value seen in Fig. 5(C)) when the environment was at 50 °C. The results of electronic impedance and photocurrent testing indicated that heat could improve the photocatalytic properties of MOF and MOF-PDA. To further confirm the contribution of heat in enhancing photocatalytic properties, DPBF was used as a detector to evaluate the yields of $^1O_2$ in an ice bath. MOF and MOF-PDA were mixed with the DPBF detector at equivalent dosages (MOF: 25 ppm; MOF-PDA: 35 ppm; PDA: 10 ppm) and exposed to light in an ice bath, where the temperature would be unable to increase. The results showed that the yields of $^1O_2$ decreased significantly in ice for both MOF and MOF-PDA, which indicated that temperature greatly influenced photocatalytic properties (Figs. 5(D–F)

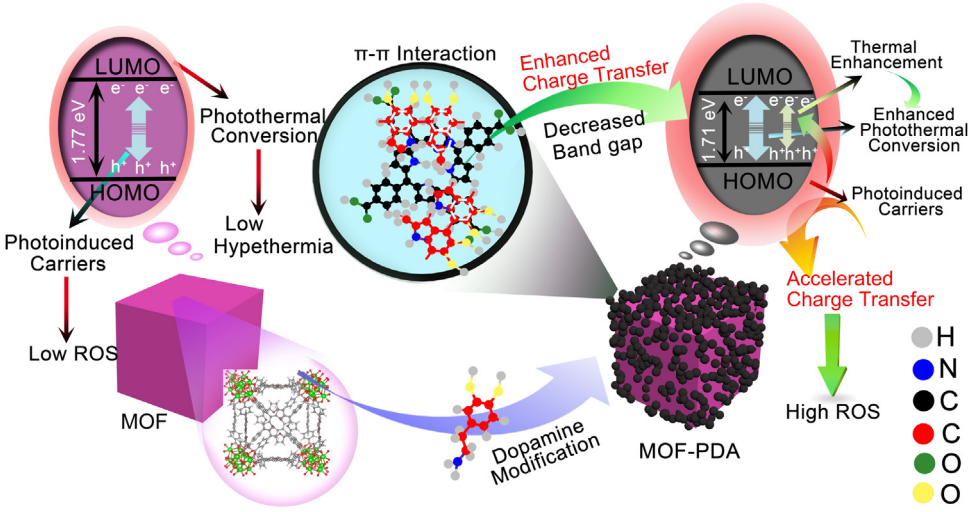

Fig. 6. Schematic illustrating the mechanism of PDA enhancing the photocatalytic property of MOF-PDA, plus the structures of MOF and MOF-PDA.

and S3), this was consistent with the implications from electronic impedance and photocurrent testing (Fig. 5(B) and (C)), since carrier mobility was affected by temperature vibrations [46,47]. Under 660 nm light irradiation, the MOF-PDA nanoparticles could produce much more heat than the pure MOF, as shown in Fig. 3, where increased carrier mobility and could lead to improved photocatalytic properties. At the same time, a higher temperature could also help with the indirect transition [46,47], which also improved the photocatalytic properties (Fig. 6). And, finally, the ability to absorb light was another factor that affected the photocatalytic properties, and MOF-PDA could absorb much more light than the MOF alone, which also greatly enhanced $^1O_2$ production.

3.4. Antibacterial property of MOF-PDA nanoparticles

To verify the nanoparticles' antibacterial properties, two kinds of bacteria were chosen as representative models; *Staphylococcus aureus* (*S. aureus*) and *Escherichia coli* (*E. coli*). As shown in Fig. 7, when the bacteria were mixed with MOF-PDA at the final dosage of 350 ppm, and exposed to 660 nm light for 20 min (0.7 W/cm^2), the antibacterial ratio could reach 99.62 % and 99.97 % for *S. aureus* and *E. coli*, respectively. For the MOF and PDA at equivalent dosages, their antibacterial ratio could reach only 34.01 %, 17.34 % for *S. aureus* and 38.21 %, 26.85 % for *E. coli*, which indicated that the antibacterial capabilities of MOF-PDA were much better than both MOF and PDA alone. Such significantly higher efficiency in killing bacteria was consistent with the enhanced photothermal and photocatalytic properties of MOF-PDA. At the same time, the results also showed that without light irradiation, all groups completely failed to kill the bacteria, as only negligible decreases in colonies were found when the bacteria were mixed with MOF, MOF-PDA, and PDA in the dark (Fig. 7). It was also apparent that aside from exposure to light, the antibacterial abilities of MOF and MOF-PDA also relied on their dosages, for both *S. aureus* and *E. coli*. When the dosage of MOF, MOF-PDA, and PDA decreased, their antibacterial properties under light irradiation significantly decreased (Figs. S4, S5). MOF-PDA could efficiently kill bacteria when exposed to 660 nm light for 20 min at the dosage of 350 ppm with the temperature reaching no higher than 55 °C, which could be safely used on skin tissue for brief periods [48]. But when the dosage decreased to 210 and 280 ppm, the antibacterial ratio under light irradiation could reach no more than 60 %. Thus, in the following experiments, MOF-PDA was used at the dosage of 350 ppm and MOF and PDA were used at dosages of 250 ppm and 100 ppm respectively without special instructions.

3.5. Antibacterial mechanism

The ANS and ONPG were used as detectors to evaluate the integrity of the bacterial membrane after the bacteria had been mixed with nanoparticles and exposed to light at different conditions. If and when the bacterial membrane broke, the ANS could bind to the hydrophobic membrane region, significantly increasing fluorescence [49]. ONPG would simultaneously react with excurrent β-galactosidase through enzymolysis and increase OD (405 nm) [50–52]. Compared against MOF (Fig. 8(A)), when the bacteria (both *S. aureus* and *E. coli*) were mixed with MOF-PDA and irradiated at room temperature for 20 min, the intensity of the fluorescence of ANS significantly increased (Fig. 8(B)), indicating the serious damage incurred by the bacterial membrane.

However, when the experiment was done in the ice bath, the temperature could not increase, fluorescence intensity increased at a much lower rate compared to that at room temperature. The results indicated that temperature was crucial for the antibacterial properties of MOF-PDA, though $^1O_2$ alone could also damage the bacteria membrane. For the MOF alone, the situation was similar. But for the PDA alone (Fig. 8(C)), when the mixture was exposed neither to light at room temperature nor in an ice bath, the fluorescence intensity hardly changed much, indicating that the PDA alone was unable to efficiently kill the bacteria itself. The results of ONPG suggested similar tendencies, when the MOF-PDA was added into the bacteria solution and then irradiated by light at room temperature, the corresponding OD was the highest in value (Fig. 8(G), (H)), followed by the bacterial solution mixed with MOF-PDA and exposed to light in an ice bath, and finally the bacterial solution mixed with MOF-PDA and kept in the dark. This result demonstrated that when the bacteria were mixed with MOF-PDA and irradiated by light in ice bath, the damage to the membrane was slighter, which indicated that the photothermal properties were important for MOF-PDA to kill bacteria, though the $^1O_2$ alone could also break the bacterial membrane. For the MOF, the result was similar, where the OD was the highest when the mixture was exposed to light at room temperature, followed by the mixture exposed to light in an ice bath, indicating that the combination of heat and $^1O_2$ could cause the most serious damage to the bacterial membrane, followed by $^1O_2$ alone. The result of PDA showed that PDA

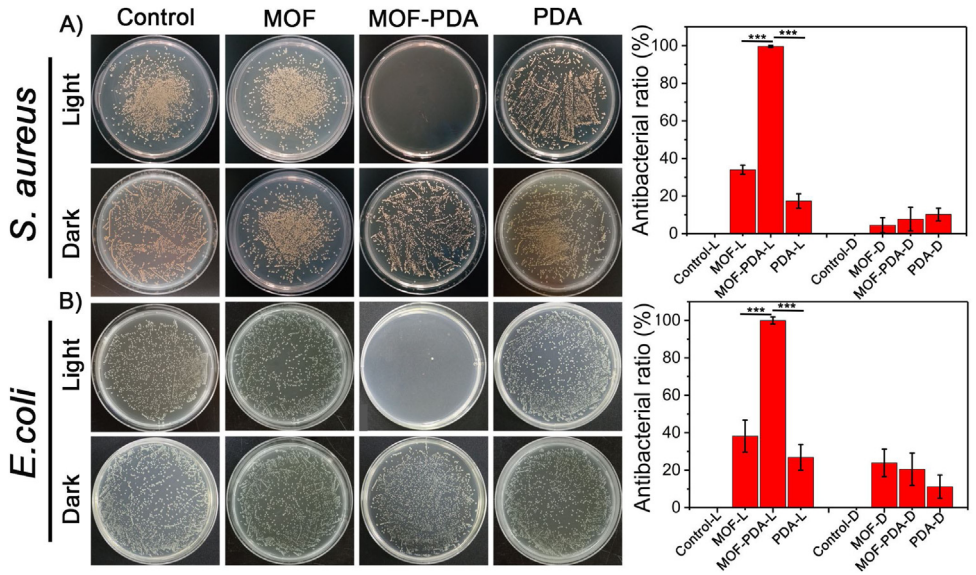

Fig. 7. Characterization of nanoparticles' antibacterial properties. A) the plate spreading results of the *S. aureus* mixed with MOF, MOF-PDA, and PDA, exposed to 660 nm light irradiation (0.7 W/cm^2) or kept in dark, and statistic analysis of the spreading results, B) the plate spreading results of the *E. coli* mixed with MOF, MOF-PDA and PDA, and exposed to 660 nm light irradiation (0.7 W/cm^2) or kept in dark, and statistic analysis of the spreading results. (dosage: MOF-PDA, 350 ppm; MOF, 250 ppm; PDA, 100 ppm).

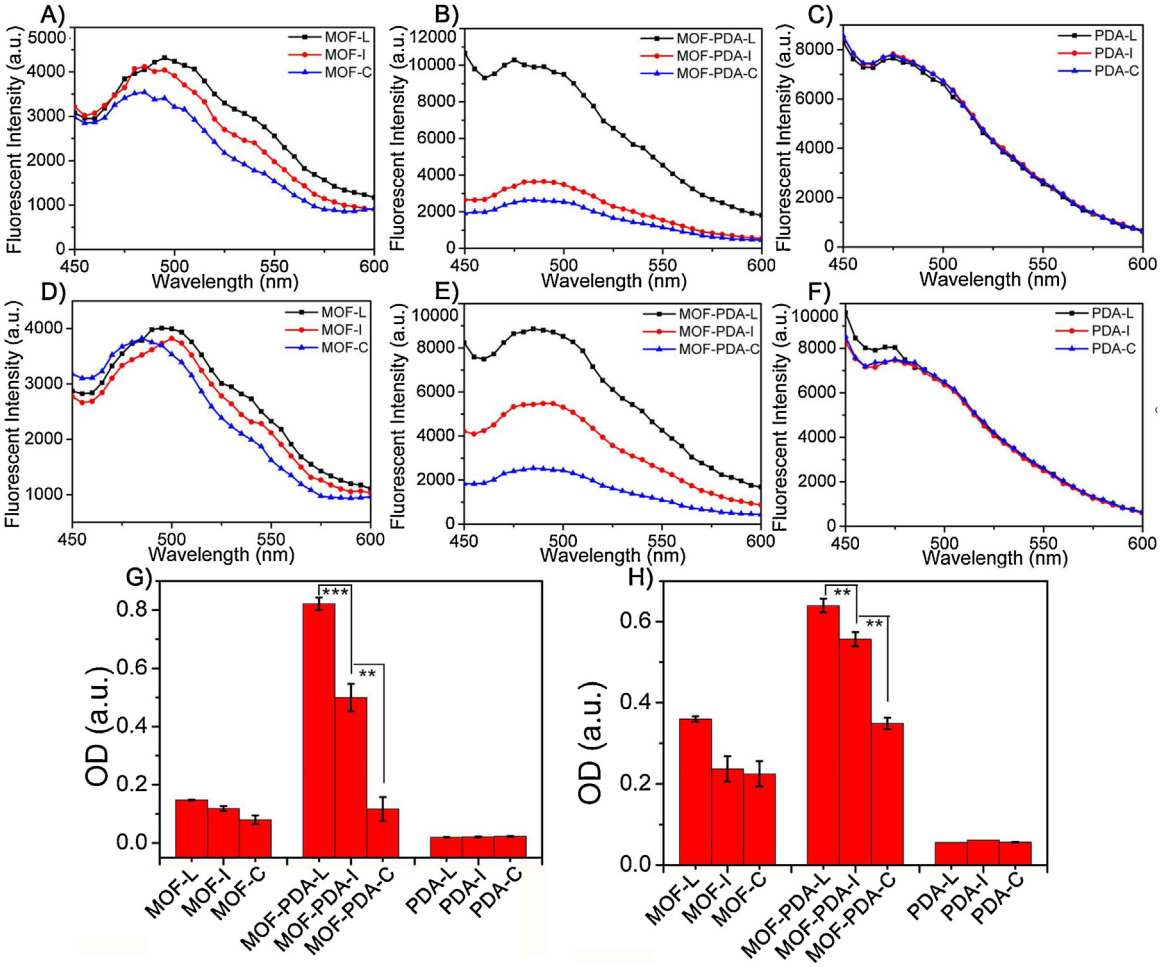

Fig. 8. Detection of bacterial membrane integrity using ANS and ONPG. After adding ANS, the *S. aureus* were mixed with A) MOF, B) MOF-PDA, C) PDA and exposed to 660 nm light or kept in the dark; after adding ANS, the *E. coli* were mixed with D) MOF, E) MOF-PDA, F) PDA and exposed to 660 nm light or kept in the dark, After the bacteria were mixed with MOF, MOF-PDA, and PDA, and exposed to 660 nm light or kept in the dark, the ONPG was added, G) *S. aureus*, H) *E. coli*.(-L termed as the mixture was exposed to light at room temperature; -I termed as the mixture was exposed to light in ice bath; -C termed as the mixture was kept in the dark throughout).

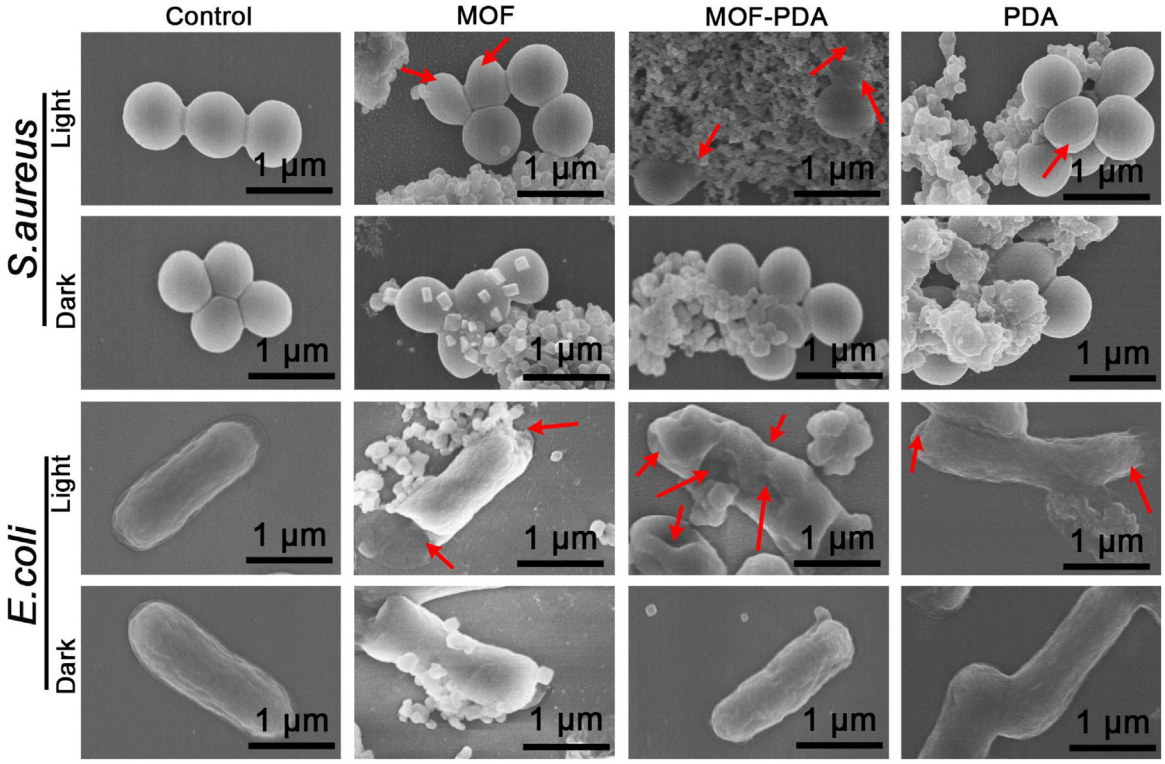

Fig. 9. SEM images of the different bacteria after different treatment. (dosage: MOF-PDA, 350 ppm; MOF, 250 ppm; PDA, 100 ppm).

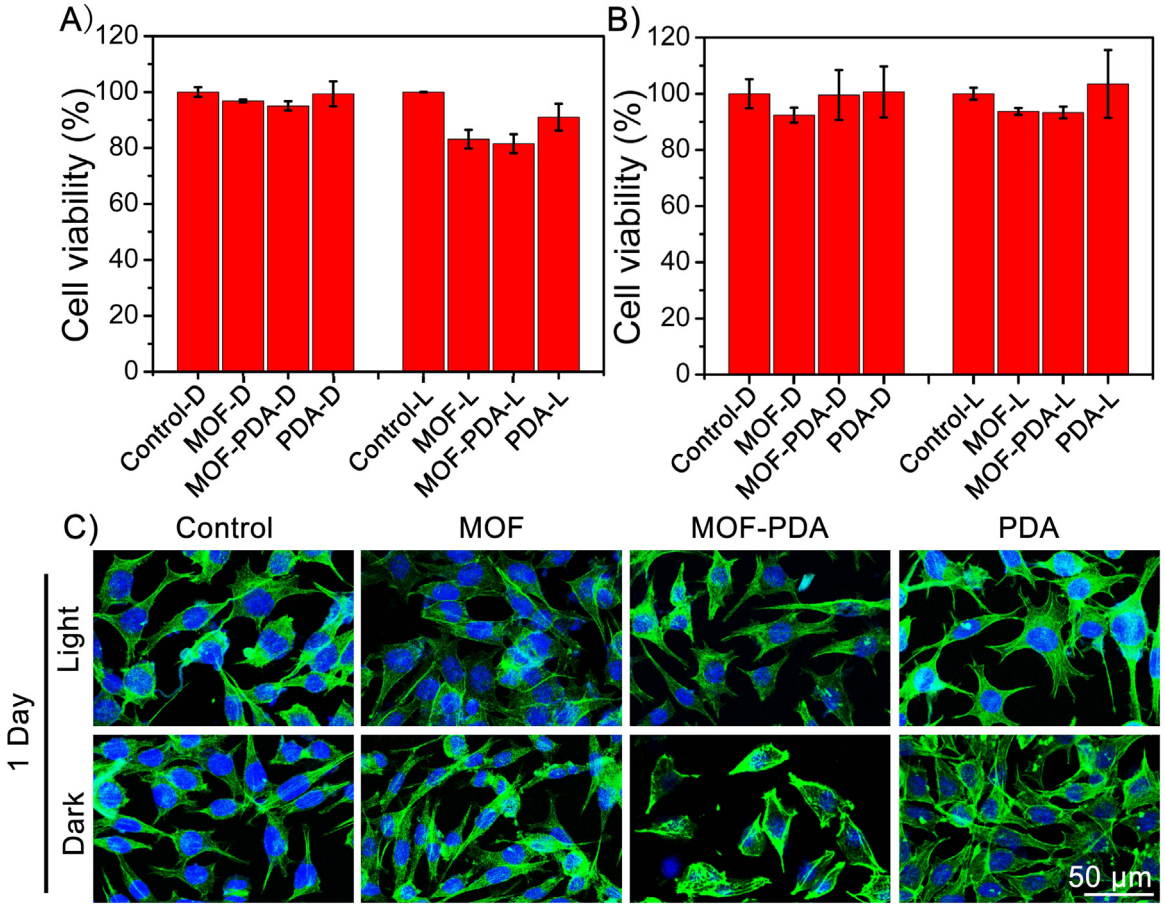

Fig. 10. Cytotoxicity of the MOF, MOF-PDA and PDA. MTT results of the NIH 3T3 cells mixed with different nanoparticles and either exposed to light or not exposed to light for: A) 1 day, B) 3 day. C) Fluorescent staining of the cells mixed with different nanoparticles and either exposed to light or kept in the dark (dosage: MOF-PDA, 350 ppm; MOF, 250 ppm; PDA, 100 ppm).

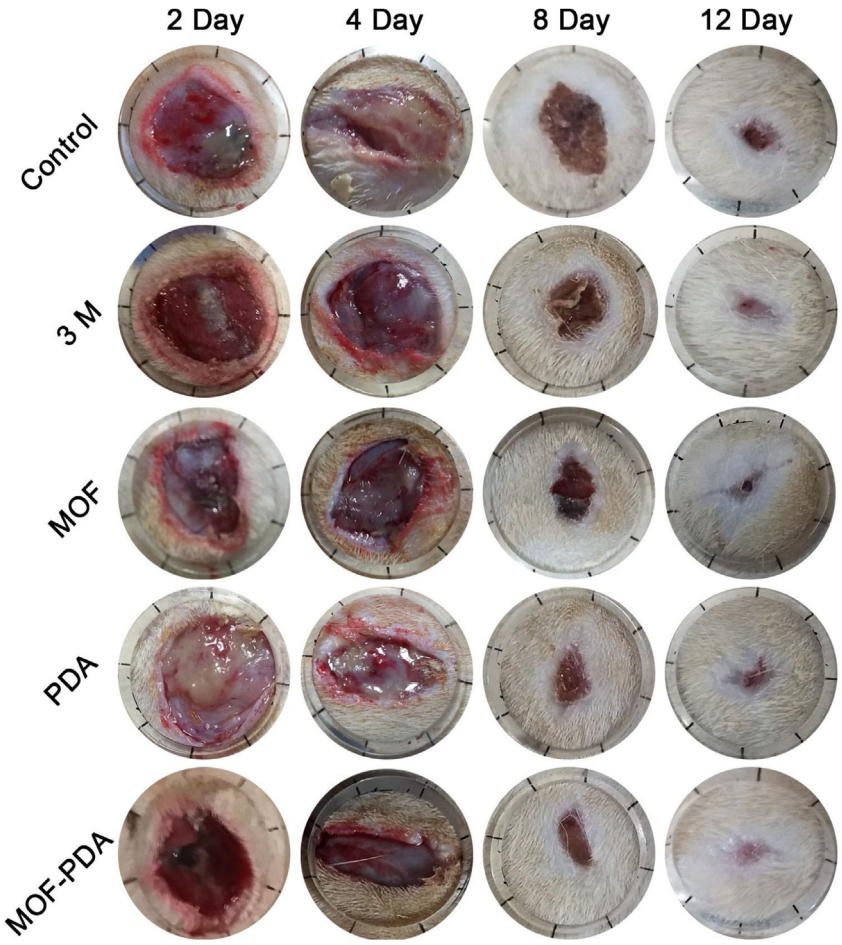

Fig. 11. The optical photographs of the infected wounds following various treatments at 2, 4, 8, 12 days. Control group, wounds covered with gauze; 3 M group, wounds covered with 3 M dressing; MOF group, wounds treated with MOF under light irradiation and covered with gauze, MOF-PDA group, wounds treated with MOF-PDA under light irradiation and covered with gauze; and then PDA group, wounds treated with PDA under light irradiation and covered with gauze.

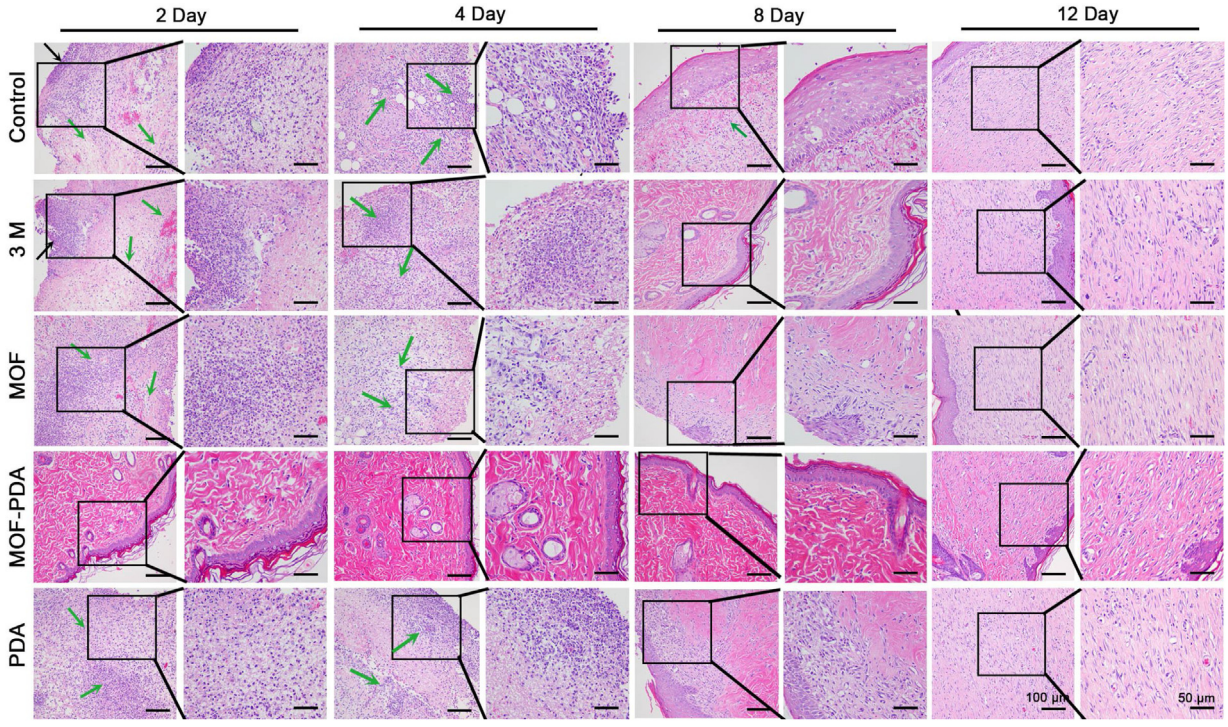

Fig. 12. H&E staining of the tissues around wounds 2, 4, 8, 12 days after treatments.

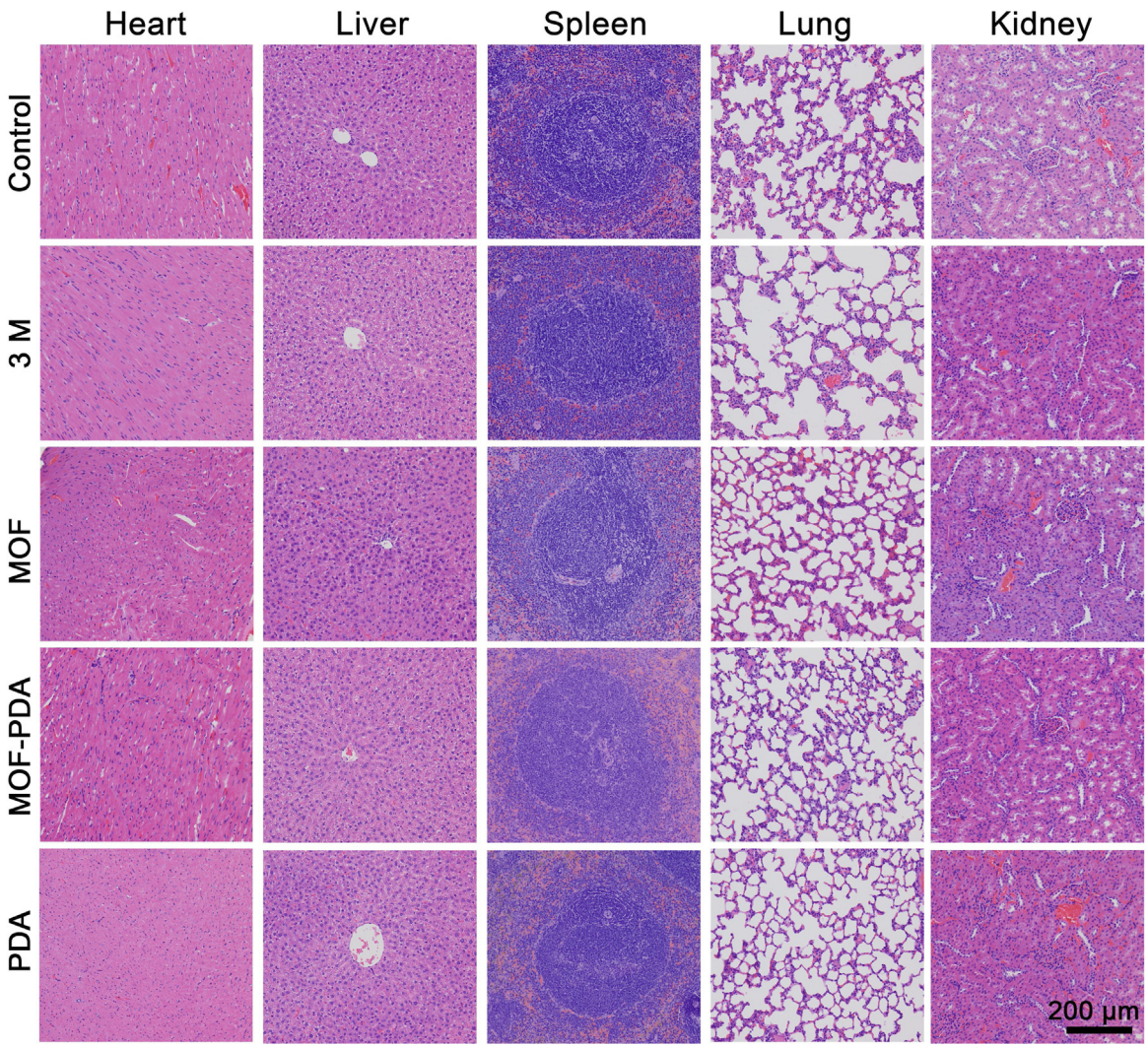

Fig. 13. H&E staining major organs of rats 12 days after treatment.

alone caused almost no change to the bacterial membrane, which is consistent with the previous results.

SEM images were captured to further determine the integrity of the bacteria after being subjected to various treatments. When all of MOF, MOF-PDA, and PDA were added into the bacteria solution and kept in the dark throughout, the morphologies of both *S. aureus* and *E. coli* remained unchanged, where the bacterial surfaces were smooth and the shapes were full of spheres or rods (Fig. 9). But when the bacteria were mixed with the MOF or MOF-PDA and exposed to light for 20 min, obvious damage was found on the membrane, marked as the red arrows in Fig. 9. Furthermore, when the MOF-PDA was added into the bacterial solution and exposed to light, the transformation of bacteria was much more serious, indicating that MOF-PDA was capable of seriously damaging bacteria.

3.6. Cytotoxicity of MOF-PDA nanoparticles

Aside from antibacterial properties, the cytotoxicity is another important property for the wound antibacterial agents [53,54]. NIH 3T3 cells were used to test the cytotoxicity of nanoparticles *in vitro* [55,56]. As the MTT results in Fig. 10(A) and (B) shown, when the nanoparticles were added into the 96-well plates and co-cultured with cells in the dark throughout (dosage: MOF, 250 ppm; MOF-PDA, 350 ppm; PDA, 100 ppm), the MOF, MOF-PDA, and PDA showed no toxicity whatsoever, even when the cells are co-cultured for three days. However, when the different nanoparticles were added to the cultured cells in the 96-well plate and exposed to light for 20 min, cells were damaged, making the cell viability of MOF and MOF-PDA around 80 %. This was because the heat and $^1O_2$ produced during light irradiation could attack the cells. The results showed that the cell viability of MOF and MOF-PDA groups were similar, which was different from the results of the bacteria killing. This might be due to the different dispersibility of MOF and MOF-PDA. Compared to MOF nanoparticles, which declined and quickly attached the bottom of the plate, the MOF-PDA nanoparticles possessed great dispersibility and could be suspended in the liquid, which resulted in a greater distance from the MOF-PDA nanoparticles to the cells at the bottom. When exposed to light, the greater distance between the MOF-PDA nanoparticles and the cells partially weakened the damage of $^1O_2$ and the heat produced, resulting in similar cell viability between the MOF and MOF-PDA groups. But in the process of killing bacteria, both the nanoparticles and the bacteria were suspended in the water, so the MOF-PDA could attach to and kill more bacteria because of the better dispersibility. Furthermore, the structure of the cells was totally different from that of the bacteria. In bacteria, many essential protein complexes are located on the cell exterior and, therefore, are accessible for inactivation by $^1O_2$. However, for eukaryocyte, the same structures are found mostly intracellularly in the mitochondrial organelles, which not only show high functional redundancy but also are very hard

for $^1O_2$ to attack [57]. After a short time, the cells could recover and begin to rapidly proliferate, as shown by the results of MTT testing after 3 days. The cell staining experiments were also performed to evaluate the cell morphologies after being cultured for 1 day. The results validated the MTT results. After the cells were co-cultured with nanoparticles in the dark for 1 day, the cells were spindle-shaped with clear cell nuclei and were well spread out, similar as with those cultured in pure medium and kept in the dark (Fig. 10(C)), which supports the excellent biocompatibility of MOF, MOF-PDA, and PDA. When the cells were mixed with nanoparticles and irradiated with light, the cell morphology did not change much; they were still spindle-shaped and well spread out, which indicated that the cells could recover soon after irradiation. All the MTT and fluorescence staining results showed that the MOF, MOF-PDA, and PDA were suitable as antibacterial agents for wound healing.

3.7. *Antibacterial properties of MOF-PDA nanoparticles* in vivo

Infected wound models were built to test the antibacterial properties of MOF-PDA *in vivo*, where 17 mm wounds were cut into the backs of the rats following treatment with anesthesia, and then bacterial solution was added. It was obvious that when the infected wounds were directly covered with gauze or 3 M dressing (the Control and 3 M groups), 2 days later, serious festering was found (Fig. 11). When the wounds were dropped with PDA or MOF and then irradiated with 660 nm light, the wounds were also infected (Fig. 11). However, when the wounds had MOF-PDA added, accompanied by light irradiation, no infection was found around the wound. Even 4 days after treatment, the wounds of the rats in the Control, 3 M, MOF, and PDA groups were still suppurative, while the wounds in the MOF-PDA group appeared to be normal without signs of infection. And 12 days later, the wounds in the MOF-PDA group were almost healed. However, the wounds in other groups were still obvious, albeit with no signs of infection. These results were consistent with those of the antibacterial experiments *in vitro*, indicating the good antibacterial properties of MOF-PDA.

Wound tissues were stained using H&E. Obviously, 2 days later, the tissues in the Control, 3 M, MOF, and PDA groups were seriously infected (Fig. 12). The corium layer was diffusely infiltrated by a large number of inflammatory cells (shown as green arrows in Fig. 12), which confirmed the serious infection of the wounds. However, for the wounds in the MOF-PDA group, the tissue was regularly arranged, with no sign of infection. After waiting for 4 days following treatment, the results of the H&E staining showed that for the Control, 3 M, MOF, and PDA groups, there were still plenty of inflammatory cells in the corium layer, and the epidermal layer was also injured, which indicated the serious infection. However, for the MOF-PDA group, the tissue was densely arranged with normal vessel distribution. After 12 days following treatment, no infection was found in the wounds of the Control, 3 M, MOF, and PDA groups, indicating that they had gradually healed. As for MOF-PDA, the tissue was healthy, with a clear structure of an epidermal layer and a corium layer (Fig. 12). This result was consistent with the photographs of wounds taken at different time points and indicated that the MOF-PDA could kill bacteria efficiently *in vivo*.

After 12 days' treatment, the major organs of the rats were extracted and stained with H&E staining. Compared with the major organs of rates in the Control and 3 M groups, no histopathological changes could be found in the major organs of rates in the MOF, MOF-PDA, and PDA groups. Furthermore, no pathological features, such as cardiomyocytes disordered infiltration, inflammatory cells scattering distribution in liver tissue and the renal interstitial hyperemia, are found in tissues of rats in MOF, MOF-PDA and PDA groups. The results indicated that the MOF-PDA showed no biotoxicity (Fig. 13).

4. Conclusion

This paper has presented the designs for an MOF-PDA hybrid material, which exhibited enhanced photothermal and photocatalytic properties due to the unique interaction between PDA and MOF. The π-π interaction and charge transfer between the PDA and H_4TCPP in MOF, which might lead to a shift in the HOMO and LUMO, leading to a decreased energy band gap and stronger photocatalytic properties of nanoparticles. Both the PDA and H_4TCPP absorbed light because of the π-π* transition. After modification, π-π interaction was observed between the PDA and H_4TCPP, and the material's π-conjugation was elongated, leading to the enhanced light absorbance of nanoparticles. At the same time, due to the extra heat produced under irradiation, the carrier mobility was improved, which also helped with the photocatalytic properties of MOF-PDA. Because of the improved photothermal and photocatalytic properties, MOF-PDA could efficiently kill bacteria (antibacterial ratio for *S. aureus* and *E. coli* was 99.62 % and 99.97 % respectively). Furthermore, the synthesized MOF-PDA showed no cytotoxicity to cells, guaranteeing their potential as antibacterial agents.

Acknowledgements

This work is jointly supported by the National Science Fund for Distinguished Young Scholars51925104, National Natural Science Foundation of China nos. 51871162, 51671081, and 51801056, the National Key Research and Development Program of China2016YFC1100600 (subproject 2016YFC1100604), Natural Science Fund of Hubei Province, 2018CFA064, RGC/NSFC (N_HKU725-1616), Hong Kong ITC (ITS/287/17, GHX/002/14SZ), as well as Health and Medical Research Fund (No. 03142446).

Appendix A. Supplementary data

Supplementary material related to this article can be found, in the online version, at doi:https://doi.org/10.1016/j.jmst.2020.05.055.

References

[1] M.X. Ma, X.M. Liu, L. Tan, Z.D. Cui, X.J. Yang, Y.Q. Liang, Z.Y. Li, Y.F. Zheng, K.W.K. Yeung, S.L. Wu, Biomater. Sci. 7 (2019) 1437–1447.
[2] Y.J. Xi, Y. Wang, J.Y. Gao, Y.F. Xiao, J.Z. Du, ACS Nano 13 (2019) 13645–13657.
[3] L. Piddock, Nat. Rev. Microbiol. 15 (2017) 639–640.
[4] J.M. Zhang, Y.H. Sun, Y. Zhao, Y.L. Liu, X.H. Yao, B. Tang, R.Q. Hang, Rare Metals 36 (2019) 552–560.
[5] X.H. Chen, Q. Wei, J.D. Hong, R. Xu, T.H. Zhou, Rare Metals 38 (2019) 413–419.
[6] H.F. Xu, G. Zhu, B.M. Hao, J. Mater. Sci. Technol. 35 (2019) 100–108.
[7] H. Deng, C.J. Doonan, H. Furukawa, R.B. Ferreira, J. Towne, C.B. Knobler, B. Wang, O.M. Yaghi, Science 327 (2010) 846–850.
[8] Z.W. Ma, J.X. Zou, D. Khan, W. Zhu, C.Z. Hu, X.Q. Zeng, W.J. Ding, J. Mater. Sci. Technol. 35 (2019) 2132–2143.
[9] B. Huang, L. Tan, X.M. Liu, J. Li, S.L. Wu, Bioact. Mater. 4 (2019) 17–21.
[10] E.L. Zhang, S. Fu, R.X. Wang, H.X. Li, Y. Liu, Z.Q. Ma, G.K. Liu, C.S. Zhu, G.W. Qin, D.F. Chen, Rare Metals 36 (2019) 476–494.
[11] L. Shi, L.Q. Yang, H.B. Zhang, K. Chang, G.X. Zhao, T. Kako, J.H. Ye, Appl. Catal. B 224 (2018) 60–68.
[12] Y. Luo, X.M. Liu, L. Tan, Z.D. Cui, X.B. Feng, X.J. Yang, Y.Q. Liang, Z.Y. Li, S.L. Zhu, Y.F. Zheng, K.W.K. Yeung, C. Yang, X.B. Wang, S.L. Wu, ACS Central Sci. 5 (2019) 1591–1601.
[13] P. Miao, G.J. Guan, H. Deng, B. Han, C. Tian, J.Y. Zhuang, Y.Y. Xu, W.Z. Liu, Z. Lin, Environ. Sci. Nano 6 (2019) 207–215.
[14] J. Park, Q. Jiang, D.W. Feng, L.Q. Mao, H.C. Zhou, J. Am. Chem. Soc. 138 (2016) 3518–3525.
[15] D. Feng, W. Chung, Z. Wei, Z. Gu, H. Jiang, Y. Chen, D.J. Darensbourg, H.C. Zhou, J. Am. Chem. Soc. 135 (2013) 17105–17110.
[16] C.J. Ou, Y.W. Zhang, D. Pan, K.K. Ding, S.C. Zhang, W.J. Xu, W.J. Wang, W.L. Si, Z. Yang, X.C. Dong, Mater. Chem. Front. 3 (2019) 1786–1792.
[17] S.Y. Li, H. Cheng, W.X. Qiu, L. Zhang, S.S. Wan, J.Y. Zeng, X.Z. Zhang, Biomaterials 142 (2017) 149–161.
[18] Q.L. Zou, M. Abbas, L.Y. Zhao, S.K. Li, G.Z. Shen, X.H. Yan, J. Am. Chem. Soc. 139 (2017) 1921–1927.

[19] A. Carangelo, A. Acquesta, T. Monetta, Bioact. Mater. 4 (2019) 71–78.
[20] D. Sharma, W.K. Jia, F. Long, S. Pati, Q.H. Chen, Y.B. Qyang, B. Lee, C.K. Choi, F. Zhao, Bioact. Mater. 4 (2019) 142–150.
[21] J.J. Feng, P.P. Zhang, A.J. Wang, Q.C. Liao, J.L. Xi, J.R. Chen, New J. Chem. 36 (2012) 148–154.
[22] S.C. Liu, J.M. Pan, J.X. Liu, Y. Ma, F.X. Qiu, L. Mei, X.W. Zeng, G.Q. Pan,Small 14 (2018), 1703968.
[23] S.M. Yu, G.W. Li, R. Liu, D. Ma, W. Xue,Adv. Funct. Mater. 28 (2018), 1707440.
[24] T. Li, P. Hu, J.W. Li, P.T. Huang, W.J. Tong, C.Y. Gao, Colloids Surf. A Physicochem. Eng. Asp. 577 (2019) 456–463.
[25] S.X. Liu, J.L. Yang, Q. Liu, Y.J. Huang, M.Q. Kong, Q. Yang, G.G. Li, Chem. Eng. J. 363 (2019) 1–12.
[26] J. Manna, S. Akbayrak, S. Özkar, Appl. Catal. B 208 (2017) 104–115.
[27] J.W. Fu, Z.H. Chen, M.H. Wang, S.J. Liu, J.H. Zhang, J. Zhang, R. Han, Q. Xu, Chem. Eng. J. 259 (2015) 53–61.
[28] F.Y. Zhao, Y.L. Ji, X.D. Weng, Y.F. Mi, C.C. Ye, Q.F. An, C.J. Gao, ACS Appl. Mater. Interfaces 8 (2016) 6693–6700.
[29] M. Maruthapandi, M. Natan, G. Jacobi, E. Banin, J.H.T. Luong, A. Gedanken, Nanomaterials 9 (2019) 1731.
[30] B. Gao, L.H. Chen, Y.L. Zhao, X. Yan, X.Y. Wang, C.R. Zhou, Y.F. Shi, W. Xue, Eur. Polym. J. 110 (2019) 192–201.
[31] S. Sohrabi, S. Dehghanpour, M. Ghalkhani, J. Mater. Sci. 53 (2018) 3624–3639.
[32] J.H. Jiang, L.P. Zhu, L.J. Zhu, H.T. Zhang, B.K. Zhu, Y.Y. Xu, ACS Appl. Mater. Interfaces 5 (2013) 12895–12904.
[33] D.D. Wang, H.H. Wu, J.J. Zhou, P.P. Xu, C.L. Wang, R.H. Shi, H.B. Wang, H. Wang, Z. Guo, Q.W. Chen,Adv. Sci. 5 (2018), 1800287.
[34] M. Wu, Q.T. Wang, D. Zhang, N.S. Liao, L.J. Wu, A. Huang, X.L. Liu, Colloids Surf. B Biointerfaces 141 (2016) 467–475.
[35] D. Zhang, M. Wu, Y.Y. Zeng, L.J. Wu, Q.T. Wang, X. Han, X.L. Liu, J.F. Liu, ACS Appl. Mater. Interfaces 7 (2015) 8176–8187.
[36] Y. Zhang, F.M. Wang, C.Q. Liu, Z.Z. Wang, L.H. Kang, Y.Y. Huang, K. Dong, J.S. Ren, X.G. Qu, ACS Nano 12 (2018) 651–661.
[37] K. Liu, R.R. Xing, C.J. Chen, G.Z. Shen, L.Y. Yan, Q.L. Zou, G.H. Ma, H. Möhwald, X.H. Yan, Angew. Chem. Int. Ed. 54 (2015) 500–505.
[38] Y.W. Ren, Y.J. Han, Z.D. Cui, X.M. Liu, Z.Y. Li, S.L. Zhu, Y.Q. Liang, S.L. Wu, Bioact. Mater. 5 (2020) 201–209.
[39] M. Tanaka, S. Hayashi, S. Eu, T. Umeyama, Y. Matano, H. Imahori, Chem. Commun. 20 (2007) 2069–2071.
[40] W.X. Lei, K.F. Ren, T.T. Chen, X.C. Chen, B.C. Li, H. Chang, J. Ji,Adv. Mater. Interfaces 3 (2016), 1600767.
[41] Z.L. Dong, H. Gong, M. Gao, W.W. Zhu, X.Q. Sun, L.Z. Feng, T.T. Fu, Y.G. Li, Z. Liu, Theranostics 6 (2016) 1031–1042.
[42] L.H. Xiao, J.H. Sun, L.B. Liu, R. Lu, H. Hu, C.G. Cheng, Y. Huang, S. Wang, ACS Appl. Mater. Interfaces 9 (2017) 5382–5391.
[43] G. Soldan, M.A. Aljuhani, M.S. Bootharaju, L.G. AbdulHalim, M.R. Parida, A.H. Emwas, O.F. Mohammed, O.M. Bakr, Angew. Chem. Int. Ed. 55 (2016) 5749–5753.
[44] Q. Hao, S.M. Hao, X.X. Niu, X. Li, D.M. Chen, H. Ding, Chin. J. Catal. 38 (2017) 278–286.
[45] X. Yu, H.L. Fan, L. Wang, Z.X. Jin, Angew. Chem. Int. Ed. 53 (2014) 12600–12604.
[46] Z.X. Gan, X.L. Wu, M. Meng, X.B. Zhu, L. Yang, P.K. Chu, ACS Nano 8 (2014) 9304–9310.
[47] X.Z. Wang, Y.R. He, Y.W. Hu, G.R. Jin, B.C. Jiang, Y.M. Huang, Sol. Energy 170 (2018) 586–593.
[48] L. Tan, J. Li, X.M. Liu, Z.D. Cui, X.J. Yang, S.L. Zhu, Z.Y. Li, X.B. Yuan, Y.F. Zheng, K.W.K. Yeung, H.B. Pan, X.B. Wang, S.L. Wu,Adv. Mater. 30 (2018), 1801808.
[49] L. Schnaider, S. Brahmachari, N.W. Schmidt, B. Meusa, S. Shaham-Niv, D. Bychenko, L. Adler-Abramovich, L.J.W. Shimon, S. Kolusheva, W.F. DeGrado, E. Gazit, Nat. Commun. 8 (2017) 1–10.
[50] T. Galbadage, D.D. Liu, L.B. Alemany, R. Pal, J.M. Tour, R.S. Gunasekera, J.D. Cirillo, ACS Nano 13 (2019) 14377–14387.
[51] K.D. LaCourse, S.B. Peterson, H.D. Kulasekara, M.C. Radey, J. Kim, J.D. Mougous, Nat. Microbiol. 3 (2018) 440–446.
[52] W. Hu, C. Li, J. Dai, H. Cui, L. Lin, Ind. Crops Prod. 130 (2019) 34–41.
[53] X.K. Ding, S. Duan, X.J. Ding, R.H. Liu, F.J. Xu,Adv. Funct. Mater. 28 (2018), 1802140.
[54] K. Kanagamani, P. Muthukrishnan, K. Saravanakumar, K. Shankar, A. Kathiresan, Rare Metals 38 (2019) 277–286.
[55] X.M. Dai, Q.Q. Guo, Y. Zhao, P. Zhang, T.Q. Zhang, X.G. Zhang, C.X. Li, ACS Appl. Mater. Interfaces 8 (2016) 25798–25807.
[56] X.L. Ye, X.M. Qin, X.R. Yan, J.K. Guo, L.H. Huang, D.J. Chen, T. Wu, Q.S. Shi, S.Z. Tan, X. Cai, Chem. Eng. J. 304 (2016) 873–881.
[57] V. Alt, T. Bechert, P. Steinrücke, M. Wagener, P. Seidel, E. Dingeldein, E. Domann, R. Schnettler, Biomaterials 25 (2004) 4383–4391.